Available online at www.sciencedirect.com
SciVerse ScienceDirect
Ceramics International 39 (2013) 1623–1629
CERAMICS INTERNATIONAL
www.elsevier.com/locate/ceramint

Reaction sequence and electrochemical properties of lithium vanadium oxide cathode materials synthesized via a hydrothermal reaction

Kyungho Kim[a], Su Han Park[a], Tae Hyung Kwon[a], Hyungkeun Ahn[b], Yang Dam Eo[a], Man-Jong Lee[a,*]

[a]Department of Advanced Technology Fusion, Konkuk University, 1 Hwayang-dong, Kwangjin-gu, Seoul 143-701, Republic of Korea
[b]Department of Electrical Engineering, Konkuk University, 1 Hwayang-dong, Kwangjin-gu, Seoul 143-701, Republic of Korea

Received 11 June 2012; received in revised form 1 August 2012; accepted 1 August 2012
Available online 11 August 2012

Abstract

Lithium vanadium oxide ($Li_{1+x}V_3O_8$) cathode materials were synthesized via a simple hydrothermal reaction followed by heat treatment at 300 or 400 °C. From both XRD and TG/DTA analyses, a detailed comprehensive reaction sequence for the formation of single-phase LiV_3O_8 is proposed. $Li_{1+x}V_3O_8$ ($x=0.2$) materials with different thermal histories show clear differences in morphologies and sizes, although they maintained an impurity-free single phase regardless of thermal treatment. Samples that were heat treated at 300 °C show an agglomerated particle shape with many nanorod-like $Li_{1+x}V_3O_8$ particles over the surface that enhance the surface area of the particles. In contrast, samples treated at 400 °C have a bi-modal particle size distribution with improved crystallinity. Such differences in morphologies clearly influence the electrochemical properties. LiV_3O_8 cathode materials that were treated at 300 and 400 °C showed initial discharge capacacities of 346.52 and 261.23 mA h/g, respectively, and discharge capacities of 78.66 and 157.35 mA h/g, respectively, after 100 cycles. The improved cyclability of LiV_3O_8 cathode materials that were heat treated at 400 °C is due to their increased crystallinity and structural stability.

Keywords: A. Powders: chemical preparation; E. Electrodes: cathode; E. Batteries; LiV_3O_8

1. Introduction

Lithium vanadium oxide (LiV_3O_8) has been extensively studied for use as a cathode material in rechargeable lithium batteries due to its attractive electrochemical properties including high specific energy, good rate capacity, long cycle life, facile preparation, and low cost [1,2]. LiV_3O_8 has a layered structure composed of two basic structural units: VO_6 octahedra and VO_5 distorted trigonal bipyramids [3]. The lithium ions that occupy the octahedral sites are linked to the V_3O_8 layer by strong ionic bonds, which impart stability to the crystal structure of LiV_3O_8 during the discharge/charge process [4]. Based on theoretical calculations, approximately 3 Li^+ (ca. 280 mA h/g) can be reversibly inserted/extracted into/from the crystalline LiV_3O_8 cathode [5]. An amorphous LiV_3O_8 cathode indicated a capacity of 419 mA h/g through the reversible insertion of a maximum 4.5 Li^+ [5]; this capacity is much higher than that of $LiCoO_2$ cathodes (140 mA h/g). In addition, LiV_3O_8 is used as both a cathode material for non-aqueous recharge lithium batteries [6,7] and an anode material for aqueous rechargeable lithium batteries (ARLB) [8–10]. In comparison to conventional lithium batteries, ARLBs have many advantages including high ion conductivity compared to non-aqueous lithium ion cells, high rate capability, and relatively high energy and power densities; they are also inherently safe even when misused and do not pollute the environment [11].

Since the electrochemical properties of LiV_3O_8 materials have been reported to be highly dependent on the preparation conditions and the resulted morphology changes, numerous techniques have been applied to elucidate such relationships to improve capacity and stability. Generally, solid-state synthesis requires a large amount of thermal energy (>680 °C) and a long reaction time (>10 h); it is

*Corresponding author. Tel.: +82 2 2049 6021; fax: +82 2 452 3410.
E-mail address: leemtx@konkuk.ac.kr (M.-J. Lee).

0272-8842/$ - see front matter
http://dx.doi.org/10.1016/j.ceramint.2012.08.004

also difficult to accurately control the Li/V ratio due to the evaporation of the Li sources, which induces a specific capacity loss of LiV_3O_8 [3]. Thus, a variety of techniques have been developed to overcome the drawbacks of conventional solid-state synthesis of LiV_3O_8. These include a sol–gel process [12–14], a hydrothermal process [15,16], freeze-drying [17], spray drying [18,19], a rheological phase reaction method [20], an ultrasonic method [21,22], a flame pyrolysis method [23], a low-heat solid-state method [24], a microwave sol–gel method [25,26], an EDTA sol–gel method [27], and a surfactant-assisted polymer precursor method [28]. Among these techniques, the hydrothermal method is most attractive to industry owing to its facile and cost-effective formation of advanced materials.

Although it has been reported that the formation of LiV_3O_8 undergoes a complex reaction sequence depending on the synthesis techniques used [29–32], the exact reaction sequence during hydrothermal reaction and subsequent heat treatment has not been detailed yet. To elucidate the complex reaction mechanism, the overall mechanism has been determined in this study by considering each step during the hydrothermal reaction and subsequent heat treatment. Furthermore, the effect of different thermal histories on the morphology and electrochemical properties of single-phase LiV_3O_8 is discussed. It has been found the heat treatment temperatures significantly affect the morphology, crystallinity, specific surface area, and electrochemical properties of the samples.

2. Experimental

2.1. Material synthesis and characterization

Analytically pure LiOH (99%+, Sigma-Aldrich), V_2O_5 (99%, Sigma-Aldrich), and NH_3H_2O (1 mol/L, Junsei, Japan) were used as raw materials without any purification. First, LiOH and V_2O_5 (Li:V = 1, 1.2:3; atomic ratio) were added to distilled water under magnetic stirring at room temperature; LiOH dissolved completely in distilled water, but V_2O_5 remained partially undissolved. To fully dissolve V_2O_5 in the distilled water, $NH_3 \cdot H_2O$ (1 mol/L) was added during stirring until pH 9 was reached. At pH 9, the reaction solution changed from brown to dark green. The solution was then transferred into a Teflon-lined stainless steel autoclave (120 mL capacity). The mixture was subjected to hydrothermal conditions at a temperature of 200 °C for 12 h. After the hydrothermal reaction, the solution became colorless and the pH of solution returned to seven. The solution was dried at 100 °C in air until a bright brown gel appeared. The gel was heat treated at either 300 or 400 °C for 12 h followed by passive cooling to room temperature. Finally, dark brown samples were obtained after the hydrothermal reaction followed by heat treatment at 300 (LVO300) or 400 °C (LVO400).

The crystal structures of the as-prepared and heated powders were determined using X-ray diffraction (XRD, X'Pert pro MPD, PANalytica, generator 3 kW) with CuKα radiation. The morphologies and particle sizes of the samples were analyzed via field emission scanning electron microscopy (FE-SEM, Hitachi SU-70, resolution:1.0 nm guaranteed or better at 15 kV acc). Thermogravimetry/differential thermal analysis (TG/DTA) was performed using a thermal analysis system (TG/DTA, SDT Q600).

2.2. Electrochemical measurements

The working electrode was prepared by pressing a mixture of the active cathode material, conductive material (super p carbon black), and binder (polyvinylidene fluoride (PVDF)) at a weight ratio of 80:15:5. The mixtures were dissolved in 1-methyl-2-pyrrolidinone (NMP) to form slurries and then uniformly cast on thick aluminum foil (thickness 0.01 mm, 99.9% trace metals basis). Li metal foil was used as the reference electrode. The electrolyte (Solvent Company, Korea) was 1 M $LiPF_6$ dissolved in a 1:1 (volume) mixture of ethylene carbonate (EC) and diethyl carbonate (DEC). The test cells (CR2016 coin-type) were assembled under a high purity argon atmosphere in a glove box (M. O. Tech, Korea) using a separator (polypropylene 2600). The discharge/charge tests were performed at room temperature using an automatic battery tester system (WBCS 3000, WonATech, Korea). Discharge/charge measurements were performed in the voltage range of 1.8–4.0 V at various current densities (0.1 and 0.2 C).

3. Result and discussion

3.1. Reaction sequence of lithium vanadium oxide

In this study, single-phase LiV_3O_8 cathode materials were synthesized using hydrothermal techniques followed by heat treatment at an elevated temperature. The first step involves the dissolution of the LiOH and V_2O_5 precursors in distilled water at room temperature, which initiates the following reactions [32]:

$$2LiOH + V_2O_5 \rightarrow 2LiVO_3, \tag{1}$$

$$2LiVO_3 + 2V_2O_5 \rightarrow 2LiV_3O_8. \tag{2}$$

Since V_2O_5 does not completely dissolve in the distilled water, aqueous ammonia was added to increase the pH to 9 and promote dissolution [31]. The aqueous ammonia addition also induces the instant formation of NH_4VO_3 (Eq. (3)), which plays an important role in the formation of the LiV_3O_8 phase as reported by Liu et al. [32]:

$$NH_4OH + V_2O_5 \rightarrow NH_4VO_3 + H_2O \tag{3}$$

It is evident from Eqs. (1) to (3) that after the addition of ammonia, the reaction mixture contains various components, including $LiVO_3$, LiV_3O_8, and NH_4VO_3 [30].

The reaction mixture was then transferred to a Teflon-lined autoclave and heated hydrothermally at 200 °C for 12 h. The obtained solutions were dried at 100 °C to form powders, which were analyzed by XRD (Fig. 1a).

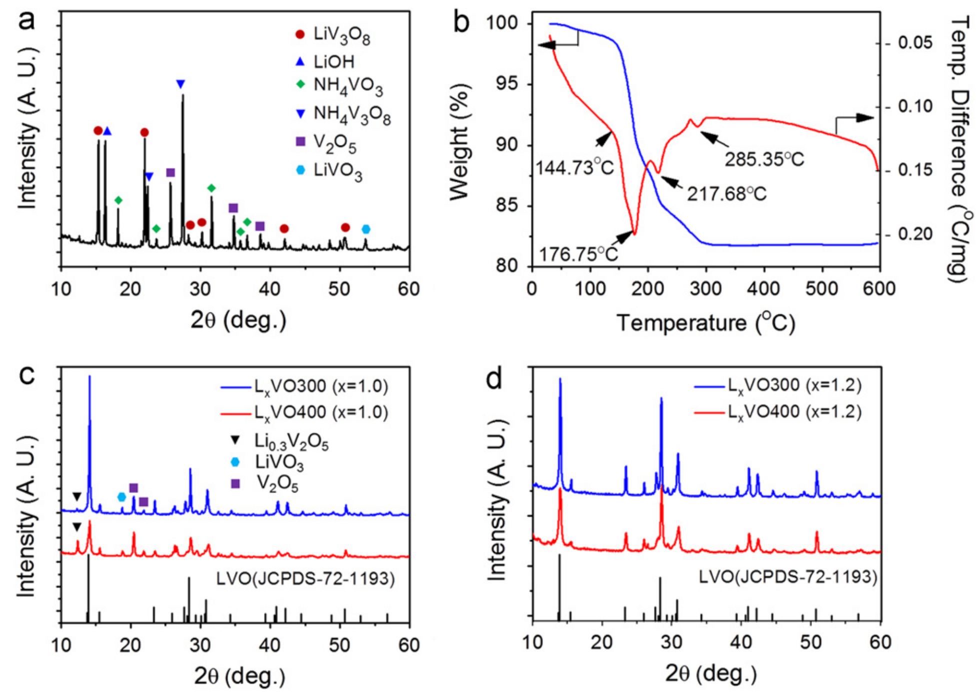

Fig. 1. (a) XRD pattern after the hydrothermal reaction, (b) TG/DTA results of samples up to 600 °C, (c) XRD patterns of $Li_{1+x}V_3O_8$ ($x=0$) samples after heat treatment at 300 and 400 °C, and (d) XRD patterns of $Li_{1+x}V_3O_8$ ($x=0.2$) samples after heat treatment at 300 and 400 °C.

The powders contain a variety of compounds including NH_4VO_3, $NH_4V_3O_8$, $LiVO_3$, LiV_3O_8, V_2O_5, and LiOH. Thus, the following reactions are possible during the hydrothermal reaction:

$$x\text{LiOH}+x\text{NH}_4\text{VO}_3\rightarrow x\text{LiVO}_3+x\text{LiOH}+\text{NH}_4 \quad (4)$$

$$x\text{LiVO}_3+x\text{V}_2\text{O}_5\rightarrow x\text{LiV}_3\text{O}_8 \quad (5)$$

$$x\text{NH}_4\text{VO}_3+x\text{V}_2\text{O}_5\rightarrow x\text{NH}_4\text{V}_3\text{O}_8 \quad (6)$$

Even after the hydrothermal reaction, the samples showed mixed crystal phases with a highest intensity peak corresponding to the intermediate $NH_4V_3O_8$ phase. Since $NH_4V_3O_8$ easily transforms to LiV_3O_8 in the presence of lithium ions through the removal of NH_4, it might play an important role in the formation of single-phase LiV_3O_8.

To determine the ideal heat-treatment temperature for the formation of single-phase LiV_3O_8, TG/DTA measurements were performed on the dried brown gels, as shown in Fig. 1b. Thermal decomposition of the precursor can be divided into three temperature stages. In the first stage, from room temperature to 150 °C, a weight loss of ~3 wt% was detected with no obvious peaks on the DTA curve. Above 150 °C, weight loss increased rapidly with increasing temperature. A considerable weight loss (14.94%) was observed in the range 150–290 °C, which indicates active combustion and decomposition of the precursor. At this stage, endothermic peaks were found at 176.75, 217.68, and 285.35 °C, as shown in Fig. 1b, which correspond to the evaporation of residual water, chemically bound water, and NH_4, respectively. In the last stage from 290 to 600 °C, little weight loss was observed. An endothermic peak at 600 °C in the DTA curve indicates total oxidation of vanadium to V^{5+} [29].

The results of XRD analyses of the dried brown gels heat treated at 300 and 400 °C to synthesize single-phase LiV_3O_8 are shown in Fig. 1c and d. Phase analysis of the samples with a stoichiometric composition (Li/V$=1/3$) (Fig. 1c) revealed the presence of an impurity ($Li_{0.3}V_2O_5$) as well as intermediate phases ($LiVO_3$ and V_2O_5), which may degrade the electrochemical properties. To synthesize impurity-free LiV_3O_8, samples with an excess of lithium ($Li_{1+x}V_3O_8$, $x=0.2$) were prepared; the XRD results shown in Fig. 1d reveal no evidence of a second phase. From the XRD analyses (Fig. 1d), a possible reaction sequence for the formation of impurity-free LiV_3O_8, which is similar to that proposed by Yang et al. [31], is as follows:

$$x\text{LiOH}+x\text{NH}_4\text{VO}_3\rightarrow x\text{LiVO}_3\cdot x\text{H}_2\text{O}+(x-y)\text{H}_2\text{O}\uparrow+\text{NH}_4\uparrow \quad (7)$$

$$x\text{LiVO}_3\cdot x\text{H}_2\text{O}+x\text{NH}_4\text{VO}_3\rightarrow \text{LiV}_3\text{O}_8+x\text{NH}_3\uparrow+(x+y)\text{H}_2\text{O}\uparrow \quad (8)$$

$$x\text{NH}_4\text{V}_3\text{O}_8\cdot x\text{H}_2\text{O}+x\text{LiOH}\rightarrow x\text{LiV}_3\text{O}_8+x\text{NH}_3\uparrow+(x+y)\text{H}_2\text{O}\uparrow \quad (9)$$

$$x\text{LiVO}_3+x\text{V}_2\text{O}_5\rightarrow \text{LiV}_3\text{O}_8 \quad (10)$$

The TG/DTA studies provide evidence of the evaporation of residual H_2O, chemically bound H_2O, and NH_4 from the precursor, as shown in Eqs. (7)–(9). According to Eq. (10), single-phase LiV_3O_8 can be synthesized above 300 °C without forming a second phase of $Li_{0.3}V_3O_8$, as shown in Fig. 1d. The overall reaction sequence is summarized in Table 1. Moreover, considering the increase of the (100) peak at 13.89° with

Table 1
Overall reaction sequence for the formation of single-phase LiV_3O_8.

	LiOH	V_2O_5	$LiVO_3$	NH_4VO_3	$NH_4V_3O_8$	LiV_3O_8
Precursors dissolution	↓	↓	O	X	X	O
Precursors (with NH_4OH)	↓	↓	↓	O	X	→
Hydrothermal reaction[a]	↓	↓	↓	↓	O (↑)	↑
Heating (< 300 °C)	↓	↓	↓	↓	↓	↑
Heating (~300 °C)	X	X	X	X	X	→

[a]200 °C for 12 h; O first formed; ↓amount decreased; ↑amount increased;→ amount constant.

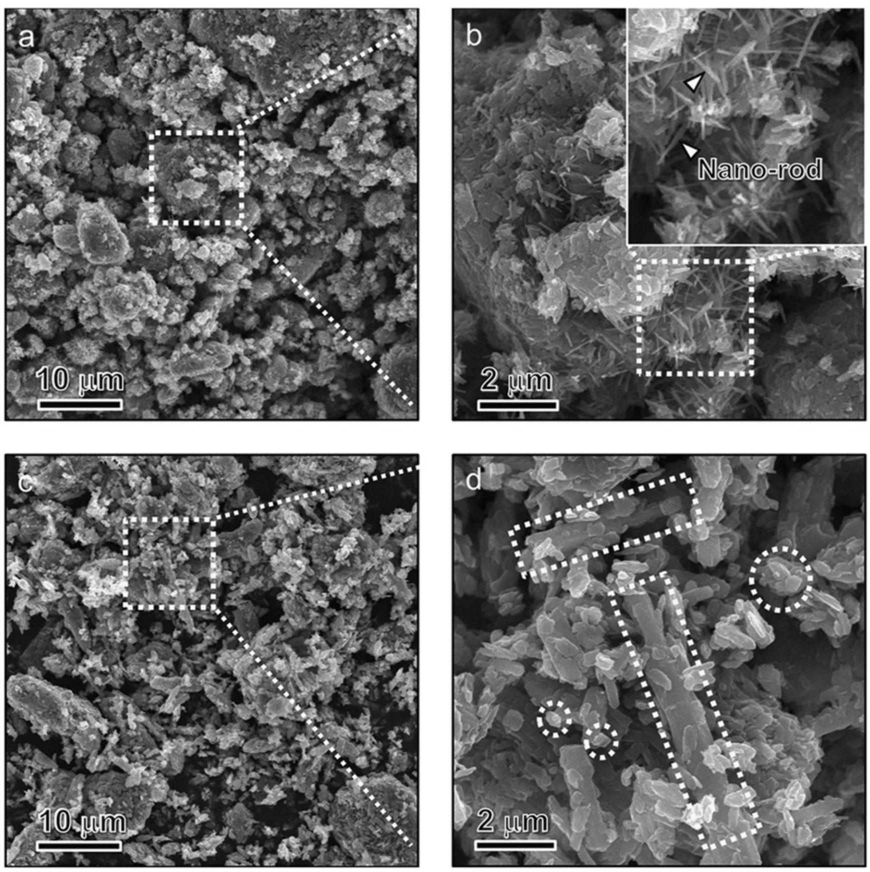

Fig. 2. SEM images of single-phase LiV_3O_8 synthesized by heat treatment at (a, b) 300 and (c, d) 400 °C. Insets in (b) show the presence of nanorods at the surface of LiV_3O_8 aggregates, and insets in (d) indicate the presence of small particles and microrods forming a bi-modal size distribution.

increasing heat-treatment temperature, it is evident that higher heat increases the crystallinity of the LiV_3O_8 phase.

3.2. The morphology of lithium vanadium oxide

Fig. 2 shows the SEM images of the single-phase LiV_3O_8 synthesized by heat treatment at 300 (Fig. 2a and b) and 400 °C (Fig. 2c and d); the morphology and size of the as-synthesized LiV_3O_8 is significantly influenced by the heat-treatment temperature. LiV_3O_8 samples synthesized by heat treatment at 300 °C (LVO300) are highly agglomerated compared with those heat treated at 400 °C (LVO400). Interestingly, as-synthesized LVO300 contains tiny nanorods (20–50 nm in diameter and ~500 nm in length) at the surface of the agglomerated particles, which increases the surface area. In contrast, as-synthesized LVO400 shows agglomerated particles without any nanorods; instead, submicron-sized particles (200–500 nm in diameter) and a few micron-sized microrods (3–10 µm in length) form the bi-modal particle size distribution. Generally, upon increasing the heat treatment temperature from 300 to 400 °C, the particles of the products become larger and more crystallized, which is in agreement with the XRD results; however, the surface area shows the reverse trend.

3.3. Electrochemical performance of lithium vanadium oxide

To investigate the effect of different heat-treatment temperatures on the electrochemical behavior of LiV_3O_8 during Li^+ insertion/extraction, the discharge–charge behavior and differential capacity (dQ/dV) characteristics of the LiV_3O_8 cathode materials were measured at a current density of 0.1–0.2 C at room temperature at a potential ranging between 1.8 and 4.0 V (vs. Li/Li^+), as shown in Fig. 3. In Fig. 3a and b, the initial capacities (Fig. 3a) and differential capacities (Fig. 3b) of LVO300 and LVO400 measured at 0.1 C are shown; LVO300 showed a higher initial capacity (Fig. 3a) and the reduction/oxidation peaks of the first cycle were significantly different with different heat-treatment temperatures (Fig. 3b). The initial discharge capacities of LVO300 and LVO400 were 346.52 and 261.23 mA h/g, respectively. A possible reason for this significant difference is the large interface area of LVO300, which is similar to that reported previously [33]: LVO300 samples contain relatively small aggregated particles as well as surface nanorods (see Fig. 3b), which decrease the diffusion distance for active lithium ions and increase the initial capacity [34]. From the differential capacities plot ($\Delta V = 0.02$ V) shown in Fig. 3b, Li insertion/extraction during the first discharge/charge process is evident. Oxidation/reduction peaks of LVO300 were found at 2.29/2.43, 2.56/2.66, 2.72/2.74, and 2.80/2.84 V, whereas those for LVO400 were found at 2.52/2.74, 2.72/2.78, and 2.80/2.88 V. During the initial discharge/charge process, the major oxidation/reduction peak (2.56/2.66 V) of LVO300 was intense compared with that (2.52/2.74 V) of LVO400, which demonstrates the higher initial capacity of LVO300.

After Li^+ insertion/extraction for 50 cycles, another 50 discharge/charge cycles were performed on the same samples at a current density of 0.2 C. Fig. 3c and d shows the variation of the 51th capacities (Fig. 3c) and differential capacities (Fig. 3d) of LVO300 and LVO400 measured at 0.2 C. In contrast with the first cycle at a current density of 0.1 C, the discharge/charge capacities (163.60/167.29 mA h/g) of LVO400 were much larger than those (103.64/106.87 mA h/g) of LVO300. Meanwhile, the main oxidation/reduction peak of LVO300 shifted from 2.56/2.66 V for the first cycle at 0.1 C to 2.53/2.72 V for the 51st cycle at 0.2 C (Fig. 3b), whereas the main peak of LVO400 did not change (Fig. 3d). The oxidation/reduction peak shift of LVO300 can be correlated to fading capacities and structural damage in the active materials during the insertion and extraction of Li ions [35]. Also, the differential capacity of LVO400 was bigger, which confirms a higher capacity, and new oxidation and reduction peaks were observed at 3.27, 3.31 and 3.75 V, and 2.12, 3.20 and 3.59 V, respectively; these contribute to the enhancement of the discharge/charge capacities of LVO400 [35].

The discharge/charge capacities and cycling performance of LiV_3O_8 cathode materials with different thermal treatment histories at two different current densities of 0.1 and 0.2 C are displayed in Fig. 4. The discharge/charge capacities (measured at 0.1 C) for the first and 50th cycles of LVO300 were 346.52/361.69 and 127.65/128.39 mA h/g, respectively; at a current density of 0.2 C, the discharge/charge capacities for the 51st and 100th cycles were 103.64/106.87 and 78.66/76.51 mA h/g, respectively. For LVO400, the discharge/charge capacities (measured at 0.1 C) for the first and 50th cycles were 261.23/263.71 and 192.50/

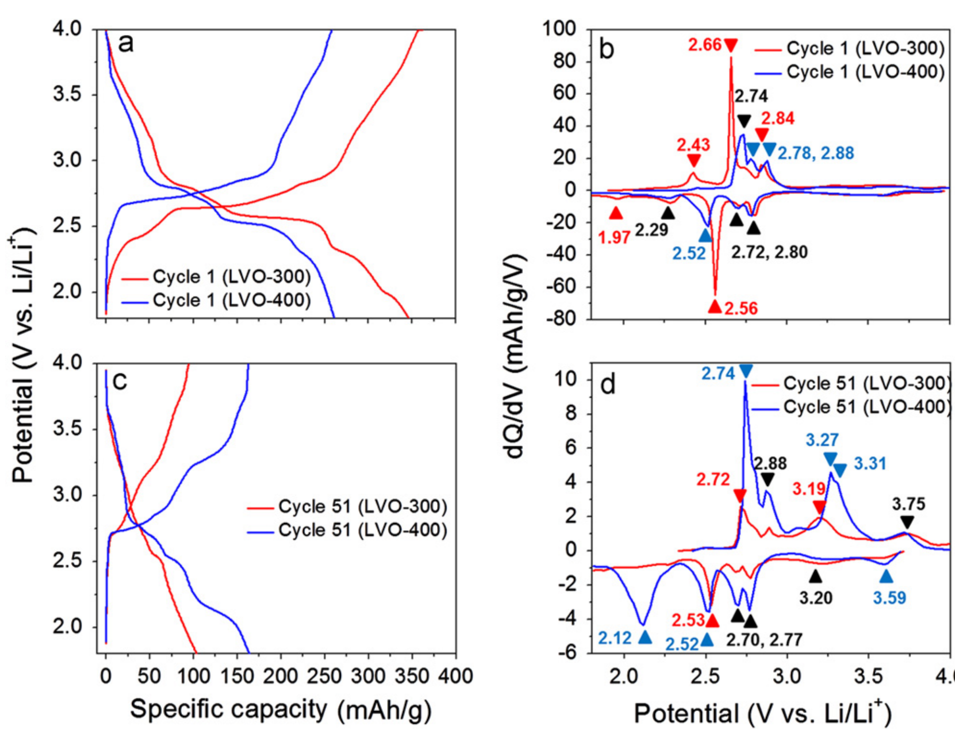

Fig. 3. Discharge–charge behaviors at the (a) first and (b) 51st cycles and differential capacity (dQ/dV) characteristics at the (c) initial and (d) 51st cycles of the LiV_3O_8 cathode materials measured at current densities of 0.1 C (a, b) and 0.2 C (c, d) at room temperature at a potential ranging between 1.8 and 4.0 V (vs. Li/Li^+).

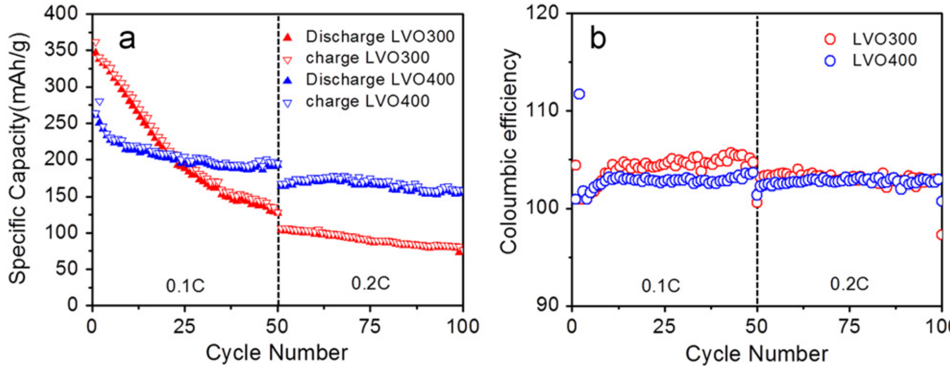

Fig. 4. (a) Cycling performance and (b) Coulombic efficiencies of LiV_3O_8 cathodes heat treated at 300 and 400 °C.

195.16 mA h/g, respectively; at a current density of 0.2 C, the discharge/charge capacities for the 51st and 100th cycles were 163.60/167.29 and 157.35/158.51 mA h/g, respectively. Although LVO300 shows higher initial capacities at a current density of 0.1 C due to its large surface area, its capacity fading was much more severe up to 50 cycles due to structural instability during the discharge/charge process; the discharge/charge capacities during the subsequent 50 cycles at 0.2 C faded much more slowly, which is probably due to structural stabilization after 50 cycles at 0.1 C. For LVO400, the discharge/charge capacities as well as cycling stability are much better, as shown in Fig. 4. During the discharge/charge process at 0.1 C up to fifth cycle, the capacity faded rapidly due to instability at the interface of the active materials and electrolytes. However, after five cycles the capacities stabilized and were almost constant up to the 50th cycle. Also, during the subsequent 50 cycles at 0.2 C, excellent cycling stability was observed up to the 100th cycle. As shown in Fig. 4, all the samples showed Coulombic efficiencies slightly greater than 100% during the entire 100 cycles. Comparing these two samples, LVO400 shows lower initial capacities but improved cycling properties than LVO300 due to its higher crystallinity and bi-modal nature of particle sizes.

4. Conclusion

In this report, we elucidated the complex reaction mechanism of LiV_3O_8 phase formation during a hydrothermal reaction followed by heat treatment. Based on XRD and TG/DTA data and the heat treatment of the hydrothermally reacted gels with an Li/V ratio of 1.2, a possible reaction sequence for the formation of impurity-free LiV_3O_8 was proposed. The formation of the intermediate $NH_4V_3O_8$ phase was determined to play an important role in the formation of the LiV_3O_8 phase. We also focused on the electrochemical properties of LiV_3O_8 cathode materials with different thermal histories; the heat treatment temperatures significantly affect the morphology, crystallinity, specific surface area, and electrochemical properties of the samples. Samples treated at 300 °C show a higher initial capacity of 346.52 mA h/g owing to the increased surface area resulting from the presence of nanorods on the aggregate surface, but rapidly fading capacity due to structural instability. In contrast, samples treated at 400 °C show excellent cycling behaviors, which is probably due to its higher crystallinity and the bi-modal particle sizes.

Acknowledgments

This paper was supported by Konkuk University in 2010.

References

[1] H.Y. Xu, H. Wang, Z.Q. Song, Y.W. Wang, Y.W. Yan, M. Yoshimura, Novel chemical method for synthesis of LiV_3O_8 nanorods as cathode materials for lithium ion batteries, Electrochimica Acta 49 (2004) 249–253.
[2] C. Cheng, Z.H. Li, X.Y. Zhan, Q.Z. Xiao, G.T. Lei, X.D. Zhou, A macaroni-like $Li_{1.2}V_3O_8$ nanomaterial with high capacity for aqueous rechargeable lithium batteries, Electrochimica Acta 55 (2010) 4627–4631.
[3] M.S. Whittingham, Lithium batteries and cathode materials, Chemical Reviews 104 (2004) 4271–4301.
[4] G. Pistoia, S. Panero, M. Tocci, R.V. Moshtev, V. Manev, Solid solutions $Li_{1+x}V_3O_8$ as cathodes for high rate secondary Li batteries, Solid State Ionics 14 (1984) 311–318.
[5] M. Zhao, L.F. Jiao, H.T. Yuan, Y. Feng, M. Zhang, Study on the silicon doped lithium trivanadate as cathode material for rechargeable lithium batteries, Solid State Ionics 178 (2007) 387–391.
[6] G. Pistoia, M.L. Divona, M. Tagliatesta, Transport and equilibrium characteristics of γ-lithium vanadium bronze, Solid State Ionics 24 (1987) 103–109.
[7] G. Pistoia, M. Pasquali, M. Tocci, R.V. Moshtev, V. Manev, Lithium/lithium vanadium oxide secondary batteries: IV evaluation of factors affecting the performance of test cells, Journal of Power Sources 132 (1985) 13–25.
[8] G. Wang, L. Fu, N. Zhao, L. Yang, Y. Wu, H. Wu, An aqueous rechargeable lithium battery with good cycling performance, Angewandte Chemie—International Edition 46 (2007) 295–297.
[9] G.J. Wang, N.H. Zhao, L.C. Yang, Y.P. Wu, H.Q. Wu, R. Holze, Characteristics of an aqueous rechargeable lithium battery (ARLB), Electrochimica Acta 52 (2007) 4911–4915.
[10] G.J. Wang, H.P. Zhang, L.J. Fu, B. Wang, Y.P. Wu, Aqueous rechargeable lithium battery (ARLB) based on LiV_3O_8 and $LiMn_2O_4$ with good cycling performance, Electrochemistry Communications 9 (2007) 1873–1876.

[11] G.J. Wang, Q.T. Qu, B. Wang, S. Shi, S. Tian, Y.P. Wu, R. Holze, Electrochemical intercalation of lithium ions into LiV_3O_8 in an aqueous electrolyte, Journal of Power Sources 189 (2009) 503–506.
[12] K.P. Lee, K.M. Manesh, K.S. Kim, Synthesis and characterization of nanostructured wires (1D) to plates (3D) LiV_3O_8 combining sol–gel and electrospinning processes, Journal of Nanoscience and Nanotechnology 9 (2009) 417–422.
[13] Y.X. Gu, F.F. Jian, Facile preparation and electrochemical properties of large-scale $Li_{1+x}V_3O_8$ nanobelts, Journal of Sol–Gel Science and Technology 46 (2008) 161–165.
[14] L. Liu, L.F. Jiao, Y.H. Zhang, J.L. Sun, L. Yang, Y.L. Miao, H.T. Yuan, Y.M. Wang, Synthesis of LiV_3O_8 by an improved citric acid assisted sol–gel method at low temperature, Materials Chemistry and Physics 111 (2008) 565–569.
[15] X.L. Li, P.P. Li, M. Luo, X.Y. Chen, J.J. Chen, Controllable solvo-hydrothermal electrodeposition of lithium vanadate uniform carnation-like nanostructure and their electrochemical performance, Journal of Solid State Electrochemistry 14 (2010) 1325–1332.
[16] H.M. Liu, Y.G. Wang, K.X. Wang, Y.R. Wang, H.S. Zhou, Synthesis and electrochemical properties of single-crystalline LiV_3O_8 nanorods as cathode materials for rechargeable lithium batteries, Journal of Power Sources 192 (2009) 668–673.
[17] O.A. Brylev, O.A. Shlyakhtin, A.V. Egorov, Y.D. Tretyakov, Phase formation and electrochemical properties of cryochemically processed $Li_{1+x}V_3O_8$ materials, Journal of Power Sources 164 (2007) 868–873.
[18] M.Y. Saidi, I.I. Olsen, R. Koksbang, Investigation of the electrochemical properties of $Fe_xV_2O_5$, Solid State Ionics 82 (1995) 203–207.
[19] N. Tran, K.G. Bramnik, H. Hibst, J. Prolss, N. Mronga, M. Holzapfel, W. Scheifele, P. Novak, Spray-drying synthesis and electrochemical performance of lithium vanadates as positive electrode materials for lithium batteries, Journal of the Electrochemical Society 155 (2008) 384–389.
[20] Q.Y. Liu, H.W. Liu, X.W. Zhou, C.J. Cong, K.L. Zhang, A soft chemistry synthesis and electrochemical properties of LiV_3O_8 as cathode material for lithium secondary batteries, Solid State Ionics 176 (2005) 1549–1554.
[21] N. Kumagai, A.S. Yu, Ultrasonically treated LiV_3O_8 as a cathode material for secondary lithium batteries, Journal of the Electrochemical Society 144 (1997) 830–837.
[22] Y.M. Liu, X.C. Zhou, Y.L. Guo, Effects of reactant dispersion on the structure and electrochemical performance of $Li_{1.2}V_3O_8$, Journal of Power Sources 184 (2008) 303–307.
[23] T.J. Patey, S.H. Ng, R. Buchel, N. Tran, K. Krumeich, J. Wang, H.K. Liu, P. Novak, Electrochemistry of LiV_3O_8 nanoparticles from flame spray pyrolysis, Electrochemical and Solid State Letters 11 (2008) 46–50.
[24] J.G. Xie, J.X. Li, H. Zhan, Y.H. Zhou, Low-temperature sol–gel synthesis of $Li_{1.2}V_3O_8$ from V_2O_5 gel, Materials Letters 57 (2003) 2682–2687.
[25] F. Wu, L. Wang, C. Wu, Y. Bai, F. Wang, Study on $Li_{1+x}V_3O_8$ synthesized by microwave sol–gel route, Materials Chemistry and Physics 115 (2009) 707–711.
[26] G. Yang, G. Wang, W.H. Hou, Microwave solid-state synthesis of LiV_3O_8 as cathode material for lithium batteries, Journal of Physical Chemistry B 109 (2005) 11186–11196.
[27] Y. Zhou, H.F. Yue, V.Y. Zhang, X.Y. Deng, Preparation and characterization of LiV_3O_8 cathode material for lithium secondary batteries through an EDTA-sol–gel method, Solid State Ionics 179 (2008) 1763–1767.
[28] A. Sakunthala, M.V. Reddy, B.V.R. Chowdari, P.C. Selvin, Preparation characterization and electrochemical performance of lithium trivanadate rods by a surfactant assisted polymer precursor method for lithium batteries, Journal of Physical Chemistry C 114 (2010) 8099–8107.
[29] A. Pan, J.G. Zhang, G. Cao, C. Liang, C. Wang, Z. Nie, Nanosheet-structured LiV_3O_8 with high capacity and excellent stability for high energy lithium batteries, Journal of Materials Chemistry 21 (2011) 10077–10084.
[30] V. Manev, A. Momchilov, A. Nassalevska, A new approach to the improvement of $Li_{1+x}V_3O_8$ performance in rechargeable lithium batteries, Journal of Power Sources 54 (1995) 501–507.
[31] H. Yang, J. Li, X.G. Zhang, Y.L. Jin, Synthesis of LiV_3O_8 nanocrystallites as cathode materials for lithium ion battery, Journal of Materials Processing Technology 207 (2008) 265–270.
[32] G.Q. Liu, C.L. Zeng, K. Yang, Study on the synthesis and properties of LiV_3O_8 rechargeable lithium batteries cathode, Electrochimica Acta 47 (2002) 3239–3243.
[33] J. Xu, H. Zhanga, T. Zhang, Q. Panb, Y. Guia, Influence of heat-treatment temperature on crystal structure, morphology and electrochemical properties of LiV_3O_8 prepared by hydrothermal reaction, Journal of Alloys and Compounds 467 (2009) 327–331.
[34] S. Jouanneau, A.L.G.L. Salle, A. Verbaere, M. Deschamps, S. Lascaud, D. Guyomard, Nanosheet-structured LiV_3O_8 with high capacity and excellent stability for high energy lithium batteries, Journal of Materials Chemistry 13 (2003) 921–927.
[35] H. Liu, Y. Wang, W. Yang, H. Zhou, A large capacity of LiV_3O_8 cathode material for rechargeable lithium-based batteries, Electrochimica Acta 56 (2011) 1392–1398.